The Years of El Niño, La Niña, and Interactions with the Tropical Indian Ocean

GARY MEYERS

CSIRO Marine and Atmospheric Research, Hobart, Tasmania, and Wealth from Oceans National Research Flagship, CSIRO, North Ryde, New South Wales, Australia

PETER MCINTOSH

CSIRO Marine and Atmospheric Research, Hobart, Tasmania, Australia

LIDIA PIGOT

CSIRO Marine and Atmospheric Research, Hobart, Tasmania, and Wealth from Oceans National Research Flagship, CSIRO, North Ryde, New South Wales, Australia

MIKE POOK

CSIRO Marine and Atmospheric Research, Hobart, Tasmania, Australia

(Manuscript received 29 April 2005, in final form 7 February 2006)

ABSTRACT

The Indian Ocean zonal dipole is a mode of variability in sea surface temperature that seriously affects the climate of many nations around the Indian Ocean rim, as well as the global climate system. It has been the subject of increasing research, and sometimes of scientific debate concerning its existence/nonexistence and dependence/independence on/from the El Niño–Southern Oscillation, since it was first clearly identified in *Nature* in 1999. Much of the debate occurred because people did not agree on what years are the El Niño or La Niña years, not to mention the newly defined years of the positive or negative dipole. A method that identifies when the positive or negative extrema of the El Niño–Southern Oscillation and Indian Ocean dipole occur is proposed, and this method is used to classify each year from 1876 to 1999. The method is statistical in nature, but has a strong basis on the oceanic physical mechanisms that control the variability of the near-equatorial Indo-Pacific basin. Early in the study it was found that some years could not be clearly classified due to strong decadal variation; these years also must be recognized, along with the reason for their ambiguity. The sensitivity of the classification of years is tested by calculating composite maps of the Indo-Pacific sea surface temperature anomaly and the probability of below median Australian rainfall for different categories of the El Niño–Indian Ocean relationship.

1. Introduction

The Indian Ocean zonal dipole mode (IOD; Saji et al. 1999; Webster et al. 1999) is a basin-scale pattern of surface and subsurface temperature that seriously affects the interannual climate anomalies of many nations around the Indian Ocean rim, as well as the global climate system (Yamagata et al. 2004). When it occurs, the pattern typically reaches a peak phase during the latter part of the year, often September–October, after a rapid development during the Southern Hemisphere winter. The pattern is in a positive phase when the sea surface temperature (SST) is anomalously cool in the east and warm in the west. The equatorial winds at this time are easterlies, with the wind coupled to the SST in the sense that it blows from the cooler toward the warmer waters. Some (but not all) positive IOD events occur during the same year as El Niño, and the same can be said about negative IOD events and La Niña (Yamagata et al. 2004). This paper is concerned with developing a method that allows us to classify with a high level of certainty when the Indian Ocean patterns and the El Niño–Southern Oscillation (ENSO) patterns occur at the same time, or independently. Having found

Corresponding author address: Dr. Gary Meyers, CSIRO Marine Research, GPO Box 1538, Hobart, Tasmania 7001, Australia. E-mail: gary.meyers@csiro.au

DOI: 10.1175/JCLI4152.1

a subset of years that can be clearly classified, the implications for the Indo-Pacific SST anomaly and Australian rainfall are identified as an example of how the classification can be used.

In addition to clarifying the relationship between ENSO and IOD, a careful classification may help the climate research community reach an international consensus on a scientific definition of El Niño and La Niña. International climate experts sometimes do not agree on whether a particular year should be classified as an El Niño or not (e.g., 1994); this ambiguity has happened several times in past years. Our initial approach to this problem is to classify all the years of the twentieth century as carefully as possible using the SST data for 1876–1999 from the U.K. Hadley Centre. A classification for such a long period of time is also likely to be useful in paleoclimate research.

2. ENSO and IOD dynamics: A basis for classifying the years

ENSO is a mode of climate variability with strong coupling between the ocean and the atmosphere in the Pacific equatorial cold tongue, a spatial relative minimum of SST that extends along the Pacific equator from the coast of South America to the date line. The cold tongue is maintained by upwelling of cooler water from the thermocline caused by the divergence of directly wind-driven surface currents (McPhaden 2004). Enhanced upwelling is associated with a shallow thermocline and stronger than normal surface divergence, and it results in the cold extreme of ENSO, called La Niña. Diminished upwelling (deep thermocline and weak surface divergence, or convergence in the case of westerly winds) results in the warm extreme, the well-known El Niño. The long persistence of El Niño and La Niña is a consequence of strong, two-way, positive feedback between the ocean and atmosphere (upwelling and wind) in the cold tongue region, while the transition from El Niño to La Niña (or vice versa) is controlled by a delayed negative feedback transmitted in the depth of the thermocline (Kessler 2002; McPhaden 2004). Upwelling is the oceanic process that links the slow physics of thermocline dynamics (Rossby and Kelvin waves) to SST, giving long persistence and predictability to the climate system. The strength of upwelling in the central and eastern Pacific is an essential controlling process in the ENSO cycle, often represented by the so-called Niño-3 index (SST anomaly averaged in 5°N–5°S, 90°–150°W).

Our understanding of the dynamics of the IOD has improved rapidly in recent years and has been thoroughly summarized by Yamagata et al. (2004). Like

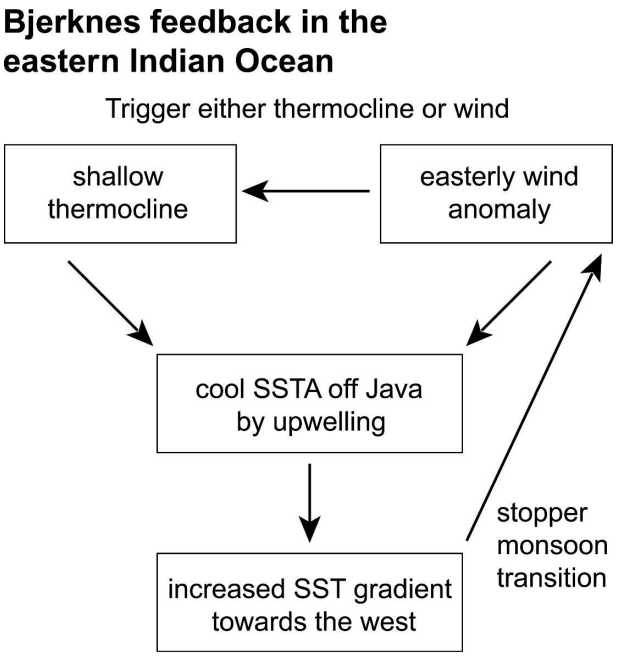

FIG. 1. Ocean–atmosphere feedbacks in the eastern Indian Ocean controlling the growth of the Indian Ocean dipole.

ENSO, the variation of subsurface temperature in the depth range of the thermocline plays an important role in the growth and maintenance of positive and negative patterns. There is evidence primarily from coupled, numerical models that the IOD can grow by ocean–atmosphere interaction involving the thermocline (Yamagata et al. 2004). Observational studies of the depth of the thermocline are fewer due to limited data coverage; nevertheless, observations have shown that the thermocline experiences large vertical displacements beneath both poles of the dipole, and the displacements are correlated to the local SST anomalies (Meyers 1996; Rao et al. 2002; Xie et al. 2002; Feng and Meyers 2003). These studies also show that as with ENSO, the depth of the thermocline is largely forced by remote winds, from both the Indian and the Pacific Oceans (Wijffels and Meyers 2004). Both remote forcing and the local wind are factors in the generation of the SST of the eastern pole (Feng and Meyers 2003), so that cool SST anomalies (i.e., positive IOD) develop when the easterly wind is favorable for upwelling along the coast of Java and the thermocline is shallow due to remote forcing. Thus, as with ENSO, upwelling in the Java–Sumatra region seems to be an essential controlling process in the growth of IOD anomalies.

The growth process is illustrated in Fig. 1 for a positive episode of the IOD. Observations and models both show that anomalies begin to grow in May, at the start of the normal upwelling season. The positive episode

can be triggered by either an anomalous shallow thermocline from remote forcing and/or an anomalous strong easterly wind along the Java coast. The triggers result in stronger than normal upwelling and locally cooler SSTs. The increased SST gradient toward the west forces an increased easterly wind, which causes further cooling. The anomalies in the eastern pole continue to grow until the monsoon transition stops the easterly wind, or remote forcing deepens the thermocline, bringing the episode to an end. An interaction between the eastern and the western regions of the Indian Ocean involving Rossby waves is also part of the growth process (Xie et al. 2002), but the focus here is on the eastern Indian Ocean. Similar growth mechanisms are described in coupled modeling studies (Gualdi et al. 2003; Annamalai et al. 2003; Yamagata et al. 2004; Cai, Hendon and Meyers 2005). In this scenario of IOD growth, like ENSO growth, upwelling is a critical process represented by the SST anomaly in the eastern pole. An index of the upwelling is the SST anomaly in the area spanning the equator to 10°S–0°, 90°–110°E, called the IODE here, which is the same area used for the eastern pole in the seminal paper by Saji et al. (1999).

3. A method of classifying the years of ENSO and IOD

The method for classifying years has to be statistical in nature; however, a purely statistical approach without considering the physical basis is not likely to work for the complex relationship between ENSO and IOD. Upwelling is a critical, physical aspect of both phenomena, as discussed above, and is selected here as a basis for the classification method. Upwelling in the Pacific cold tongue is represented by the Niño-3 region and upwelling off Java–Sumatra is represented by the IODE. They are the key time series used in the method. However, ENSO and IOD are basin-scale phenomena. Typically, the western Pacific cools when the Niño-3 area warms during El Niño, and the western Indian Ocean warms when the IODE cools during a positive episode of IOD. Two additional time series of area-averaged SST anomalies are used here to represent the basin-scale variations: NiñoWP (defined in Table 1) for the western Pacific and IODW (defined in Table 1) for the western Indian Ocean.

The four SST anomaly time series were derived from the historical SST data compiled by the Hadley Centre for 1876–1999, the so-called HadISST 1.0 dataset (Rayner et al. 2003). The areas covered by the four indices are defined in Table 1. The IODE and IODW are calculated in the same regions used by Saji et al. (1999) to form a difference index for the IOD. The Niño-3 and NiñoWP indices represent temperature differences across the Pacific. The Niño-3 index has the largest variance by more than a factor of 2 (Table 1). All four indices were therefore normalized by the standard deviation to give them equal weight in the classification method. Two additional time series were used for reasons explained below: the Southern Oscillation index (SOI) and the Darwin surface pressure obtained from the Australian Bureau of Meteorology (information online at http://www.bom.gov.au/climate/current/soihtm1.shtml). All of the time series were filtered with a 5-month running mean and normalized to have unit variance and zero mean for the period of the study.

TABLE 1. Indices of the SST anomaly.

Name	Lat	Lon	Std dev (°C)
Niño-3	5.5°S–5.5°N	150.5°–90.5°W	0.76
NiñoWP	5.5°S–5.5°N	130.5°–155.5°E	0.26
IODE	10.5°–0.5°S	90.5°–110.5°E	0.30
IODW	10.5°S–10.5°N	50.5°–70.5°E	0.33

The first step taken is to identify ENSO using the four SST anomaly indices combined with the SOI and Darwin pressure. The pressure indices are added here to be sure that a strong ENSO signal will emerge from a joint statistical analysis of all the time series. The ENSO signal appears in these indices with substantial phase lags (Yamagata et al. 2004), which complicate a straightforward empirical orthogonal function (EOF) analysis of the joint coherent variations. The phase lags are likely to spread the ENSO variance into more than one EOF (Emery and Thomson 2001). To avoid scattering, the phase lags relative to the Niño-3 index were identified by cross-correlation analysis, and removed by shifting each index to align with the Niño-3 results.

With the above arrangements of the data, an index of ENSO can be derived by simple statistics. By aligning all the time series with the Niño-3 index, we are intentionally placing emphasis on the index of upwelling in the cold tongue. After removing the phase lags, the EOF of the six indices was then calculated. The first lagged EOF accounts for 60% of the variance and the temporal coefficients clearly pick up the ENSO signal (Fig. 2, top). Its time coefficients will be used to classify the El Niño and La Niña years later in this study. The second lagged EOF (not presented) accounts for 22% of the variance and largely represents a basin-scale warming trend in the Indian Ocean since the 1950s.

It is worth mentioning here that we call the above statistical method a lagged EOF analysis. Its purpose is to avoid scattering a signal that moves in space and time into more than one EOF mode. It is similar to so-called

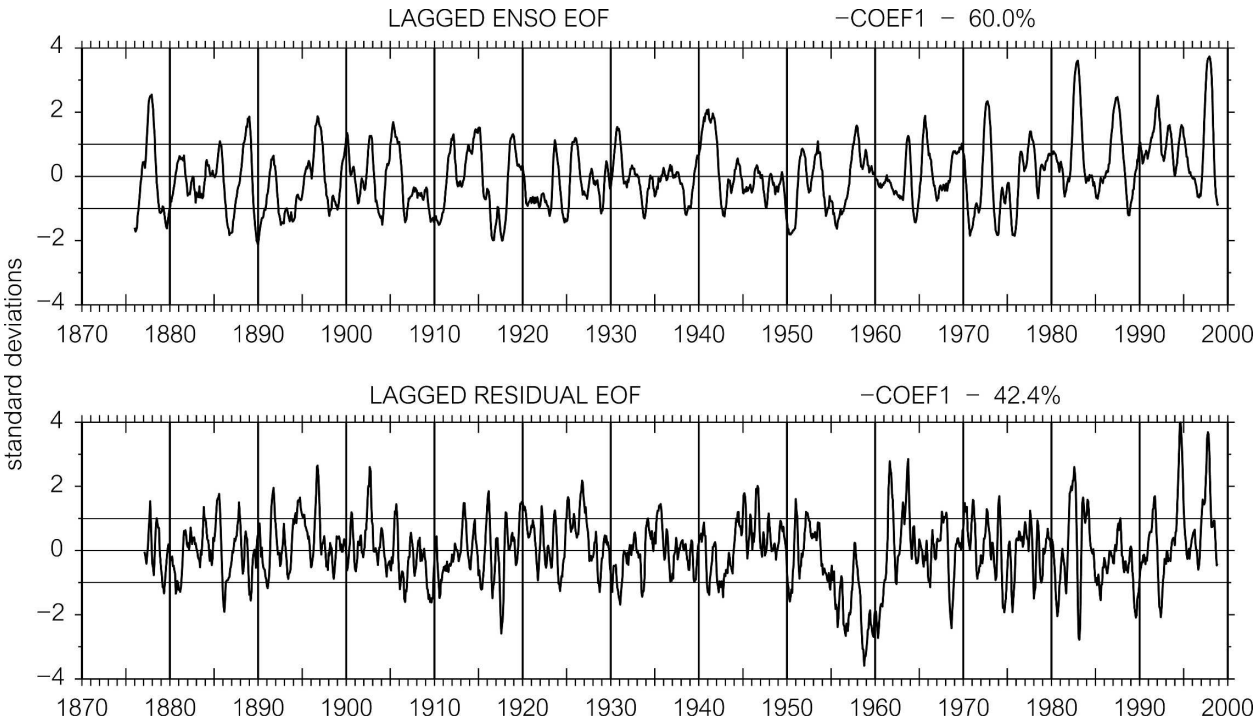

FIG. 2. Indices of the (top) ENSO and (bottom) IOD, as determined by lagged EOF analysis of the indices in Table 1.

extended EOF analysis, but it avoids repeated time series in the data matrix. It also allows us to focus the EOFs on a variable thought to be most important in the physical process, which was the index of ENSO upwelling in this case.

Now we need to derive an index of the IOD that is independent of ENSO. The ENSO signal and the trend were removed by reconstructing a time series from the first two EOFs for each input, restoring the phase lags, and subtracting the reconstructions from the original, normalized data. This leaves a set of residuals, which should have no or very little ENSO signal remaining.

The residual SST time series were used to determine the index of the IOD, using a second pass of the lagged EOF analysis. The residuals were normalized to unit variance again. The lags were removed again, relative to the IODE in this case in order to emphasize the index of upwelling off of Java–Sumatra. The lagged EOFs of the residuals were then calculated. The first EOF accounts for 42% of the residual variance. Its time coefficients (Fig. 2, bottom) are used later in the study to identify IOD episodes. The index shows recent well-known episodes of positive IOD, such as the episodes in 1961, 1994, and 1997.

In summary, the procedure was

- to identify the ENSO signal and trends by lagged EOF analysis, with a focus on upwelling in the Pacific equatorial cold tongue;
- to remove the ENSO signal and trends by reconstruction with the first two EOFs, generating a set of residual time series; and
- to identify the IOD signal by a second pass of the lagged EOF analysis of the residuals, with a focus on upwelling in the Java–Sumatra region.

4. The years of ENSO and IOD

The method in section 3 has produced indices representative of ENSO and IOD (Fig. 2). We now want to use these indices to identify the years when El Niño, La Niña, and positive or negative IOD occurred, as well as the years when these phenomena did not develop. A careful analysis of the two indices is required to achieve this for the entire twentieth century, particularly during the times when the decadal variation is strong.

It is tempting to use the ± 1 standard deviation (σ) lines shown in Fig. 2 to make this classification. However, the largest decadal variations cause uncertainty; in particular,

- the El Niño peaks trend upward in the SST anomaly after a dip around 1950;
- the La Niña troughs shift upward to a new level after 1976, without a trend; and
- the IOD index shifts downward strongly from 1954 to 1960.

TABLE 2. Classification of years when El Niño or La Niña and/or positive or negative Indian Ocean dipole occurred. Boldface (lightface) indicates a higher (lower) level of certainty in the classification as explained in the text. The classification is given lower certainty if either the ENSO phenomenon or the IOD phenomenon is not clear.

	Negative IOD	No event	Positive IOD
El Niño	**1930**	**1877**, **1888**, **1899**, **1911**, **1914**, 1918, 1925, **1940**, 1941, **1965**, **1986**, **1987**	**1896**, **1902**, **1905**, **1923**, 1957, **1963**, **1972**, **1982**, **1991**, **1997**
No event	**1880**, **1958**, **1968**, **1974**, **1980**, **1985**, **1989**, **1992**	1881, **1882**, **1883**, **1884**, **1895**, **1898**, **1901**, **1904**, **1907**, **1908**, **1912**, 1915, 1920, **1921**, **1927**, **1929**, 1931, **1932**, **1934**, **1936**, **1937**, **1939**, **1943**, **1947**, **1948**, 1951, 1952, **1953**, 1956, 1959, 1960, **1962**, **1966**, **1969**, **1976**, **1979**, **1990**, 1993, **1995**	**1885**, **1887**, **1891**, **1894**, 1900, 1913, **1919**, **1926**, **1935**, **1944**, **1945**, **1946**, **1961**, **1967**, 1977, **1983**, 1994
La Niña	**1906**, **1909**, **1910**, 1916, **1917**, **1928**, **1933**, **1942**, **1950**, **1975**, 1981	**1878**, 1879, 1886, 1889, **1890, 1892**, **1893**, **1897**, **1903**, 1922, 1924, **1938**, **1949**, 1954, 1955, **1964**, 1970, 1971, **1973**, 1978, 1984, **1988**, 1996, 1998	

Recognizing that any filtering or adjustment of values creates uncertainty in defining ENSO and IOD years, we have initially *not* classified the years during 1976–1999 and 1954–1960. The remaining years were classified when the two indices were outside the ± 1-σ lines. For El Niño and La Niña, we recognized that many episodes span the latter half and early part of consecutive years. A year was classified as El Niño or La Niña if the index in Fig. 2 was outside of ± 1 σ for at least two consecutive months during the period from June of the first year to February of the next year. The original data were filtered with a 5-month running mean so that the two consecutive months outside of 1 σ usually indicated a much longer anomaly of the same sign. Episodes that span 2 yr are named here by the first year. Similarly, the years of positive and negative IODs were identified as the years when the index in Fig. 2 was outside of ± 1 σ for 2 months during the season when the Java–Sumatra upwelling can occur (June–December). The years when the indices are inside the standard deviation are classified as no event.

The years identified in this way are summarized in Table 2 in boldface, in a format that shows when ENSO and IOD occur together, or separately. For example, the top three boxes show all the El Niño years and when they occur with a positive, negative, or no-IOD event. Similarly, the three boxes vertically aligned on the right show all the positive IOD years in boldface and when they occur with an El Niño, a La Niña or a no-ENSO event. And so forth for the other classifications.

It is useful to classify all years for some applications, so now the periods that were perturbed by the strongest decadal variations, 1954–1960 and 1976–1999, have to be addressed. We do not think that bandpass filtering is a good approach to removing decadal variation because the rapid shifts in 1954 and 1960 in the IOD index and in 1976 in the ENSO index will scatter into many frequencies, including the higher ones. Instead, we chose a much simpler approach. The shift in La Niña troughs is associated with a climatic shift in 1976 identified in many other parts of the world (Trenberth 1990; Graham 1995). We interpret the shift in La Niña troughs to represent a change in the background state on which El Niño grows. The level of post-1976 troughs was restored to the earlier level by shifting the post-1976 values downward by 0.72, the mean value of the ENSO index after 1976. The shift to align the La Niña troughs partially reduces, but does not eliminate, the upward trend in El Niño peaks. The shift in the IOD index during 1954–1960 is not a well-known climate anomaly, and needs further identification using other climate variables. Since it appears to develop and decay rapidly, in the SST data at least, it was also adjusted using a simple shift in the index. The mean during the period was -1.67. The curve was simply shifted upward by this amount.

After this adjustment to both indices, each year was classified during the periods of strong decadal variation according to the ± 1-σ levels as defined above. However, any filtering or adjustment to the indices creates some uncertainty in the classification of these years. To be conservative, we considered the classification for ENSO and IOD for a particular year to be relatively certain if it did not change in making the above adjustments. In this case, it was entered in Table 2 in boldface, indicating a higher level of certainty in the classification. If it changed, it was entered in Table 2 in lightface, indicating a lower level of certainty. Any future users of Table 2 should take these uncertainties into account, as well as any year when one or both of the indices lay close to a 1-σ line.

The classification of El Niño events after 1976 came out as follows. After shifting the ENSO index downward, the El Niño events that remained above the 1-σ line were 1982, 1986, 1987, 1991, and 1997. These years

are shown in Table 2 in boldface. The other positive peaks (1977, 1983, and 1994) changed classification after the shift. They are not called El Niño years in Table 2, but the use of lightface indicates that the classification is debatable. The year 1994 deserves special discussion. It was a very strong positive IOD event and has been used in many studies to characterize IOD episodes. The implication of this study is that 1994 is a debatable example of an event that occurred when El Niño was absent.

The La Niña events came out as follows. The La Niña event in 1988 did not change classification after the shift, and was entered in Table 2 in boldface. The other negative peaks changed classification to La Niña and were entered in Table 2 in lightface, indicating some uncertainty in the classification.

The decadal variation in the IOD index during 1954–60 was adjusted in a similar way, as discussed above. Only the negative IOD in 1958 did not change classification and was left below the 1-σ line. It was entered in Table 2 in boldface. All of the other years changed classification and were entered in Table 2 in lightface, indicating some uncertainty.

Table 2 shows that an approximately equal number of positive IOD events occurred with El Niño as without, and an approximately equal number of negative events occurred with La Niña as without. An important question is, why does El Niño sometimes occur with positive IOD and sometimes not. Annamalai et al. (2005) suggested that this may be related to decadal variation in the depth of the thermocline off of Java–Sumatra. This seems a reasonable hypothesis that can be tested in the future using ocean reanalysis products for a longer period than was available to Annamalai et al. (2005). The classification of years in Table 2 should be useful for this purpose, and also for identifying the other unique dynamics and teleconnections of dipole events that are independent of ENSO.

Table 2 also shows that a positive dipole with La Niña never occurred, and a negative dipole with El Niño occurred only once. The two empty categories are probably also a consequence of the transmission of ENSO signals in the depth of the thermocline through the Indonesian seas (Wijffels and Meyers 2004; Annamalai et al. 2005). The deep thermocline in the western Pacific during La Niña transmits to the Indonesian region and makes strong upwelling (positive IOD) highly unlikely. The shallow thermocline transmitted during El Niño makes a warm SST south of Java unlikely.

Table 2 is intended to be used in future studies of ocean–atmosphere dynamics and teleconnections during ENSO and IOD. It is tempting to use all of the years in the table to maximize the number in each category. However, when data from the years in lightface are used for a composite average for example, we should keep in mind that the classification is debatable. The result should be checked against the average for only the boldface years if possible.

In carrying out this study, we noted an interesting aspect of IOD that can be noted here, even though it is not directly relevant to the classification in Table 2. There are 23 yr when the IOD index reaches a relative maximum or minimum outside of the 1-σ lines during January–March. Upwelling off of Java–Sumatra does not occur in this season due to a prevailing westerly wind and a deep thermocline. Therefore, these are not IOD events according to our analysis of the coupled ocean–atmosphere behavior discussed in section 2. Of the 23 such occasions, 13 are positive and 10 are negative. A careful analysis of the time series in Fig. 2 shows that the positive occasions are usually the year after some El Niño's and the negative ones the year after some La Niña's. However, many El Niño's and La Niña's do not have this effect on the IOD index. Thus, the peaks early in the year are an aspect of ENSO that was not removed by the lagged EOF analysis. The 23 cases are an as yet unknown aspect of ENSO interaction with the Indian Ocean that needs further research.

5. Composite maps of SST anomaly and rainfall

An obvious use of Table 2 is to calculate composite averages of ocean–atmosphere variables. We did this for SST and rainfall to illustrate the use.

Composite maps of SST anomalies averaged for June–November (Fig. 3) were calculated for the categories of the ENSO–IOD relationship in Table 2. The composite used only the years in boldface, indicating a more certain classification. The strongest SST anomaly patterns occur for El Niño with positive IOD (Fig. 3b) and La Niña with negative IOD (Fig. 3f). The equatorial Pacific SST anomaly covers the widest band of latitude in both categories, and the Java–Sumatra upwelling zone has the strongest signal along the coast. The composites for negative IOD (Fig. 3c) and positive IOD (Fig. 3e) when there is no ENSO event show the unexpected feature that both have a slightly cooler than normal Pacific cold tongue. This was not expected for the positive IOD and consequently was checked against other commonly used SST datasets and found in them also (not presented). When El Niño or La Niña occur with no IOD event (Figs. 3a and 3g), the ENSO signal in the western tropical Pacific spreads weakly into the eastern Indian Ocean, but it does not show the upwelling or downwelling signals near Java–Sumatra that

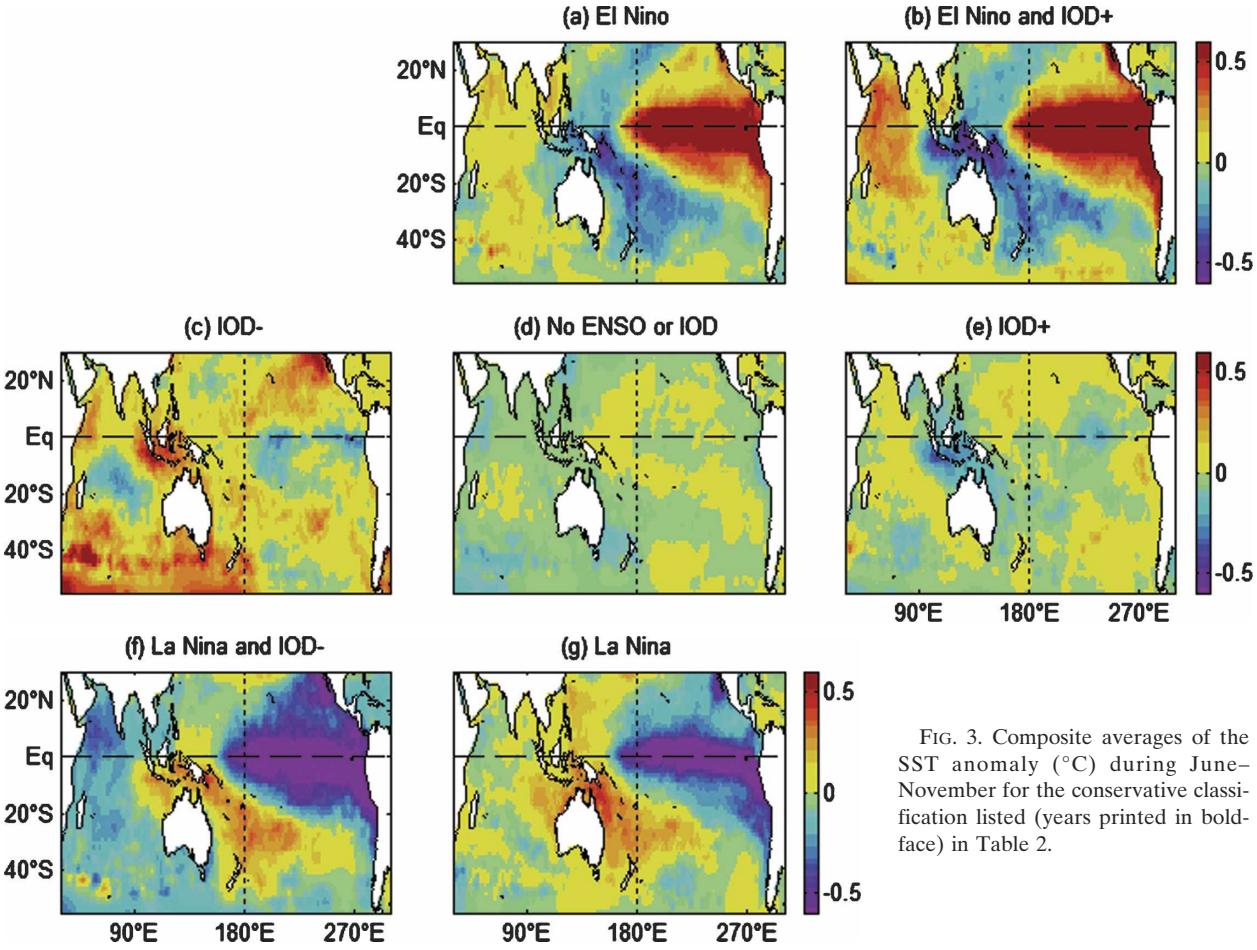

FIG. 3. Composite averages of the SST anomaly (°C) during June–November for the conservative classification listed (years printed in boldface) in Table 2.

are associated with IOD (Figs. 3c and 3e), as is expected from the analysis of the IOD dynamics in section 2. Both the expected and the unexpected features in Fig. 3 illustrate the potential usefulness of the classification in Table 2.

We also used Table 2 to show the impact of ENSO and IOD on Australian rainfall (Fig. 4). Monthly rainfall on a 0.5° grid was provided by the Australian Bureau of Meteorology. The color code represents the probability of below median rainfall (red, high probability; blue, low probability) estimated by the fraction of years in each category that had below median rainfall for the period June–November. El Niño and a positive IOD occurring together (Fig. 4b) show a high probability of low rainfall in Queensland (NE Australia). El Niño occurring by itself (Fig. 4a) has a larger portion of the continent at risk of low rainfall. The positive IOD occurring by itself (Fig. 4e) gives increased risk of low rainfall across central Australia and into the southeastern states. This pattern seems related to the so-called northwest cloud bands (Tapp and Barrell 1984; Telcik and Pattiaratchi 2001), thought to affect weather and climate in the southern part of the country. The southwestern corner of Western Australia has a high risk of low rainfall when El Niño occurs alone (Fig. 4a), and a high probability of good rainfall when positive IOD occurs alone (Fig. 4e), but a neutral condition when El Niño occurs with a positive IOD (Fig. 4b). It is particularly interesting that there are clear asymmetries in the probability patterns for El Niño with positive IOD (Fig. 4b) and La Niña with negative IOD (Fig. 4f). The changes in rainfall patterns in Fig. 4 suggest that the atmosphere over Australia is highly sensitive to small changes in the SST pattern in the oceans north of Australia, generated by ocean dynamics in both the Pacific and Indian Oceans.

The classification of El Niño and La Niña years in Table 2 needs to be compared with earlier attempts to classify years. There have been many attempts to list El Niño and La Niña years, going back to the seminal paper by Quinn et al. (1987) and updated by recent studies (e.g., Trenberth 1997), as well as lists published online by the National Oceanic and Atmospheric Administration's Climate Prediction Center (NOAA/CPC)

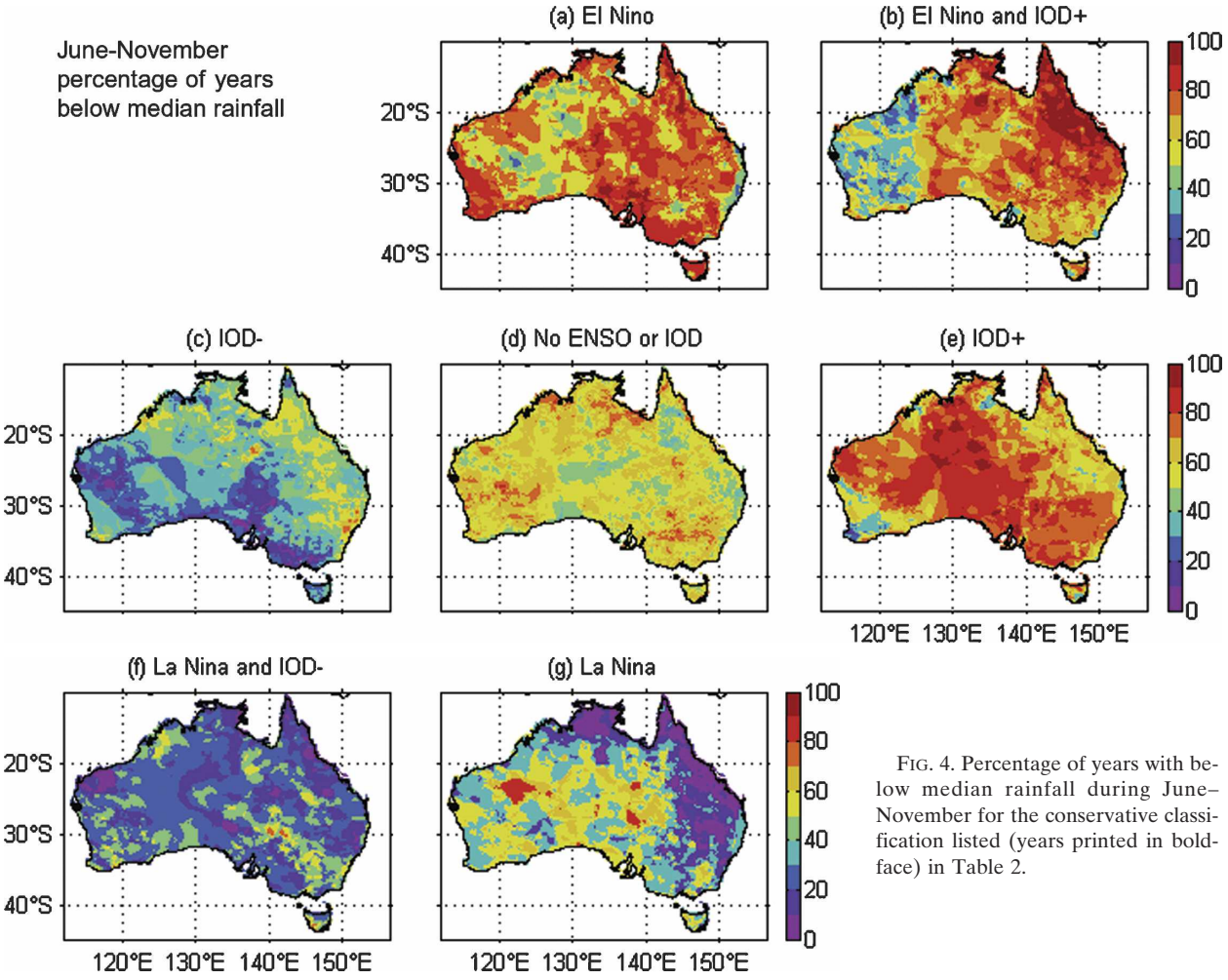

FIG. 4. Percentage of years with below median rainfall during June–November for the conservative classification listed (years printed in boldface) in Table 2.

(http://www.cpc.ncep.noaa.gov/products/analysis_monitoring/ensostuff/ensoyears.shtml) and Columbia University's International Research Institute (IRI) (http://iri.columbia.edu/climate/ENSO/background/pastevent.html#list). We have compared the classification of years in Table 2 to these lists, which cover the years after 1950. All of the years after 1950 classified as definitely El Niño or La Niña in Table 2 appear on these commonly used lists. However, the CPC, IRI, and Trenberth lists include a number of episodes classified as uncertain episodes in this study, and in some cases as not El Niño or La Niña.

Yamagata et al. (2004) prepared lists of positive and negative IOD years after 1958 using the temperature difference across the tropical Indian Ocean as the IOD index. The list agrees with the positive IOD years identified in Table 2, with the exceptions that 1983 and 1991 are not on his list. The agreement for negative IOD episodes is not good, with only the years 1958, 1989, and 1992 appearing on his list. The differences with Yamagata's tables occur because we have identified the IOD primarily on an upwelling index in the eastern Indian Ocean, while Yamagata identifies the IOD on the temperature difference across the ocean. The SST anomaly in the western Indian Ocean does not have a strong impact on the IOD index used in this study. Thus, the emphasis on a physical process—upwelling—has made a considerable difference in this case.

6. Conclusions

A recent, careful analysis of many of the indices of ENSO by Hanley et al. (2003) concluded that there is currently no consensus within the scientific community as to which of the indices best captures ENSO. At present there is no consensus on an international scientific definition of El Niño and La Niña. Consequently, some years like 1994 are called El Niño in one paper but not in another. This paper is written in the spirit of contributing to a resolution of that chal-

lenge. There are three major differences between the approach used here and those of earlier studies. First, we decided at the outset that the classification of years has to have a physical basis, chosen to be the upwelling processes for both ENSO and IOD, in addition to a statistical analysis. Second, we recognized from the outset that there will be uncertainty about some years and this needs to be expressed clearly in the classification. Third, we have tried to address the entire tropical Indo-Pacific basin, rather than focus just on the Pacific. The result (Table 2) identifies seven categories, or phases, to the ENSO–IOD relationship. Composite averages of SST and Australian rainfall show detailed and distinctive features in the different phases, in particular the occurrence (or not) of upwelling off of Java–Sumatra and the interplay of El Niño and the positive IOD in generating rainfall anomalies in southwestern Western Australia. This study highlights the need to develop a capability to predict interannual SST anomalies in the seas north of Australia in both the Pacific and the Indian Oceans. Coupled climate models are not to our knowledge successful in doing this at the present time.

Acknowledgments. This research was partially supported by the CSIRO Wealth from Oceans National Research Flagship and the South East Australia Climate Initiative. We are grateful for helpful comments from Helen Phillips, Manuel Nunez, and two anonymous referees.

REFERENCES

Annamalai, H., R. Murtugudde, J. Potemra, S. P. Xie, P. Liu, and B. Wang, 2003: Coupled dynamics over the Indian Ocean: Spring initiation of the zonal mode. *Deep-Sea Res. II,* **50,** 2305–2330.

——, J. Potemra, R. Murtugudde, and J. P. McCreary, 2005: Effect of preconditioning on the extreme climate events in the tropical Indian Ocean. *J. Climate,* **18,** 3450–3469.

Cai, W., H. H. Hendon, and G. Meyers, 2005: Indian Ocean dipolelike variability in the CSIRO Mark 3 coupled climate model. *J. Climate,* **18,** 1449–1468.

Emery, W. J., and R. E. Thomson, 2001: *Data Analysis Methods in Physical Oceanography*. Pergamon, 634 pp.

Feng, M., and G. Meyers, 2003: Interannual variability in the tropical Indian Ocean—A two-year time scale in the Indian Ocean dipole. *Deep-Sea Res. II,* **50,** 2263–2284.

Graham, N. E., 1995: Simulation of recent global temperature trends. *Science,* **267,** 666–671.

Gualdi, S. E., E. Guilyardi, A. Navarra, S. Masina, and P. Delecluse, 2003: The interannual variability in the tropical Indian Ocean as simulated by a CGCM. *Climate Dyn.,* **20,** 567–582.

Hanley, D. E., M. A. Bourassa, J. J. O'Brien, S. R. Smith, and E. R. Spade, 2003: A quantitative evaluation of ENSO indices. *J. Climate,* **16,** 1249–1258.

Kessler, W. S., 2002: Is ENSO a cycle or a series of events? *Geophys. Res. Lett.,* **29,** 2125, doi:10.1029/2002GL015924.

McPhaden, M. J., 2004: Evolution of the 2002/03 El Niño. *Bull. Amer. Meteor. Soc.,* **85,** 677–695.

Meyers, G., 1996: Variation of Indonesian throughflow and the El Niño–Southern Oscillation. *J. Geophys. Res.,* **101,** 12 255–12 263.

Quinn, W. H., V. T. Neal, and S. E. Antunez de Mayolo, 1987: El Niño occurrences over the past four and a half centuries. *J. Geophys. Res.,* **92,** 14 449–14 461.

Rao, S. A., S. K. Behera, Y. Masumoto, and T. Yamagata, 2002: Interannual variability in the subsurface tropical Indian Ocean. *Deep-Sea Res. II,* **49,** 1549–1572.

Rayner, N. A., D. E. Parker, E. B. Horton, C. K. Folland, L. V. Alexander, D. P. Rowell, E. C. Kent, and A. Kaplan, 2003: Global analyses of sea surface temperature, sea ice, and night marine air temperature since the late nineteenth century. *J. Geophys. Res.,* **108,** 4407, doi:10.1029/2002JD002670.

Saji, N. H., and Coauthors, 1999: A dipole in the tropical Indian Ocean. *Nature,* **401,** 360–363.

Tapp, R., and S. Barrell, 1984: The north-west Australian cloudband: Climatology characteristics and factors associated with development. *J. Climatol.,* **4,** 411–424.

Telcik, N., and C. Pattiaratchi, 2001: The influence of northwest cloudbands on eastern Australian rainfall. Centre for Water Research Rep. UWA23, University of Western Australia, Perth, Western Australia, Australia, 51 pp.

Trenberth, K. E., 1990: Recent observed decadal climate changes in the Northern Hemisphere. *Bull. Amer. Meteor. Soc.,* **71,** 988–993.

——, 1997: The definition of El Niño. *Bull. Amer. Meteor. Soc.,* **78,** 2771–2777.

Webster, P. J., A. M. Moore, J. P. Loschnigg, and R. R. Leben, 1999: Coupled ocean–atmosphere dynamics in the Indian Ocean during 1997–98. *Nature,* **401,** 356–360.

Wijffels, S., and G. Meyers, 2004: An intersection of oceanic waveguides—Variability in the Indonesian Throughflow region. *J. Phys. Oceanogr.,* **34,** 1232–1253.

Xie, S. P., H. Annamalai, F. A. Schott, and J. P. McCreary, 2002: Structure and mechanisms of south Indian Ocean climate variability. *J. Climate,* **15,** 867–878.

Yamagata, T., S. K. Behera, J. J. Luo, S. Masson, M. R. Jury, and S. A. Rao, 2004: Coupled ocean–atmosphere variability in the tropical Indian Ocean. *Ocean–Atmosphere Interaction and Climate Variability, Geophys. Monogr.,* Vol. 147, Amer. Geophys. Union, 189–212.